Superfluidity of lattice semions

D.L. Feder and C. Kallin
Department of Physics and Astronomy, McMaster University, Hamilton, Ontario, Canada L8S 4M1
(Received 21 November 1994)

Semions on the square, triangular, and *kagomé* lattices are studied using mean-field theory and numerical diagonalization. Semions are particles obeying fractional statistics, with statistics parameter $\nu = 1/2$. A mean-field treatment which includes Gaussian fluctuations indicates that semions on a lattice form a superfluid at zero temperature for most densities ρ. The mean-field results are compared with those of a numerical analysis of semions on small lattices. Using finite-size scaling, the lattice semions are tested for flux quantization, a signature of superfluidity. The results of the numerical analysis generally corroborate those of the mean-field approach.

I. INTRODUCTION

Quasiparticles obeying fractional statistics, anyons,[1,2] are thought to be the excitations of a number of strongly correlated electronic systems in two dimensions. The anyon excitations of $GaAs/Al_xGa_{1-x}As$ heterojunctions subjected to strong transverse magnetic fields condense into an incompressible quantum Hall fluid, leading to the experimentally observable hierarchy of stable states in the fractional quantum Hall effect.[3–5] It has been proposed that systems with magnetic frustration, such as the Heisenberg antiferromagnet on the triangular or *kagomé* lattice, may have a chiral spin-liquid ground state[6–9] which supports quasiparticles with half-Fermi statistics (semions).[10]

Hartree-Fock and random phase approximation calculations indicate that semions in the continuum form a superfluid at zero temperature in the absence of a magnetic field, or a superconductor if the semions carry charge.[11,12] For this reason, it has been suggested that semions may play a significant role in high-temperature superconductivity,[13] though there is at present no conclusive experimental evidence for the breaking of parity or time-reversal symmetry that is a fundamental characteristic of anyon models.[14–16] In any case, the novel physics of quasiparticles in two dimensions warrants a detailed study of the characteristics of anyon systems.

The ground-state properties of semions on a lattice are of particular interest. This is due to the possible relevance of fractional statistics to the aforementioned condensed matter systems, and because additional effects due to the lattice can alter the results of various approximate treatments of anyon systems. Mean-field calculations which incorporate the effect of local fluctuations[17,18] indicate that anyons on the square lattice with statistics $\nu = 1 - 1/n$ (n integer) form a superfluid at zero temperature, but only for certain lattice fillings; the lattice filling factor or density ρ must satisfy $\rho = r/q$, where r and q are mutually prime integers and q is larger than twice the common factor of r and n. The purpose of this paper is twofold: first, to determine whether these density restrictions are a spurious result of the mean-field approximation, a lattice-dependent feature, or a more universal characteristic of anyon superfluid states, and second, to more generally ascertain the validity of anyon mean-field theory.

Numerical approaches to the problem of anyons on a lattice have generally corroborated the mean-field predictions. Canright, Girvin, and Brass[19] considered anyons on a rectangular lattice with cylindrical boundary conditions. The ground-state energy of anyons in a mean-field representation compared favorably with the exact anyon ground-state energy. They also found evidence of flux quantization.[20] Wu, Kallin, and Brass[21] and Hatsugai, Kohmoto, and Wu[22] have pointed out that the periodicity of the ground-state energy with external flux for anyons on the cylinder is not sufficient indication of a superfluid state since energy level crossings between the ground state and excited states can mimic flux quantization curves. These boundary conditions also lead to significant edge and finite-size effects. Wu, Kallin, and Brass[21] eliminated edge effects by studying anyons on a sphere, but important finite-size effects persist which make an extrapolation of the ground-state properties to the thermodynamic limit difficult. Kallin[23] has examined semions ($\nu = 1/2$) on the square lattice with periodic boundary conditions in both directions. Finite-size effects were minimized by studying the size dependence of the flux quantization signature. While the results are compatible with the mean-field predictions, only a general correlation of superfluidity with semion density is made.

The present work extends the previous mean-field[17,18] and numerical[23] studies of anyons. In order to make a more careful assessment of the validity of the mean-field approach and of the density restrictions the lattice imposes on semion superfluid states, three different lattices are studied: the square, the triangle, and the *kagomé*. Since the mean-field approach predicts lattice-dependent restrictions on the superfluidity, a detailed comparison of the mean-field and numerical results for semions on various lattices should shed light on the general validity of the mean-field approximation.

In the mean-field theory, the semions are represented

by fermions attached to $\phi_0/2$ flux tubes, where $\phi_0 = hc/e$ is the flux quantum.[2,24] The flux is spread out so that there is an equal amount through each unit cell. The solution of the magnetic Bloch problem yields Landau subbands; each subband carries an integral quantum Hall conductance[25] which is a topological invariant[26] uniquely defined by the subband structure. Fluctuations of the statistical flux and of the particle density spatially follow one another, resulting in a linear collective mode, and therefore superfluidity, only for specific values of the quantum Hall conductance.[17]

In the numerical investigation, semions on small lattices with periodic boundary conditions in both directions are studied by the exact diagonalization of the Hamiltonian. The system is tested for flux quantization by monitoring the change in the ground-state energy with applied flux. It has been previously noted[27,22,23] that anyons with statistics $\nu = m/n$ on the torus will have all energies ϕ_0/n-periodic in applied flux. True flux quantization can be determined by investigating the scaling of the energy barrier, the difference between the maximum and adjacent minimum of the ground-state energy, with system size. The torus is particularly suited for an investigation of flux quantization in anyon systems since the periodicity of the ground-state energy ensures that the energy barrier is well defined.

In Sec. II, the mean-field theory for anyons on the square, triangle, and *kagomé* lattices is described in detail. The criteria for superfluidity that arise from the consideration of fluctuations about the mean-field configuration are outlined. The results of the mean-field analysis for anyons on the three lattices are given in Sec. III. It is shown that semions form a superfluid for all densities $\rho < 1/2$, but only for certain densities in the regime $\rho \geq 1/2$. In Sec. IV, the Hamiltonian employed in the numerical analysis of lattice semions is explicitly written. Section V contains the results of the flux quantization investigation for semions on the three lattices. The results of the mean-field and numerical analyses are compared and discussed in Sec. VI.

II. MEAN-FIELD THEORY

The tight-binding Hamiltonian for anyons on a lattice is

$$H = -t \sum_{\langle ij\rangle\alpha\beta} \tilde{a}^{\dagger}_{j\beta}\tilde{a}_{i\alpha}, \tag{2.1}$$

where $\tilde{a}^{\dagger}_{i\alpha}$ ($\tilde{a}_{i\alpha}$) creates (destroys) an anyon of type α (explained below) at lattice site i, and the sum is over nearest neighbors. The units are chosen so that the energy scale, t, and the lattice spacing, a, are both set to unity. The mean-field Hamiltonian is obtained by representing the anyons by fermions coupled to fractional fluxoids and spreading out the flux to form a uniform background fictitious field. This procedure leads to

$$H = -\sum_{\langle ij\rangle\alpha,\beta} c^{\dagger}_{j,\beta}c_{i,\alpha}e^{i2\pi\theta_{ij\alpha\beta}}, \tag{2.2}$$

where $c_{i,\alpha}$ destroys a fermion of type α at site i. The phase $\theta_{ij\alpha\beta}$ is defined on a lattice link by

$$\theta_{ij\alpha\beta} = \frac{1}{\phi_0}\int_{i,\alpha}^{j,\beta} \mathbf{A}\cdot d\mathbf{l}, \tag{2.3}$$

where $\mathbf{A}$ is the vector potential associated with the average background flux per unit cell Φ. If the field is directed normal to the lattice along the $\hat{z}$ direction, the Landau gauge can be chosen to define the vector potential

$$\mathbf{A} = \Phi(0, x, 0). \tag{2.4}$$

The average flux per unit cell is given by[17]

$$\Phi = \phi_0(1-\nu)\lambda\rho \equiv \phi_0\frac{P}{Q}, \tag{2.5}$$

where ν is the statistical phase ($\nu = 1/2$ for semions), ρ is the particle density, and λ is the ratio of lattice sites to unit cells. The integers P and Q have no common factors.

A. Magnetic Bloch electrons

The square, triangular (Fig. 1), and *kagomé* (Fig. 2) lattices are considered. The unit cell is chosen to be a square for the square lattice and a rhombus for both the triangle and *kagomé* lattices. The unit cell of the square and triangular lattices contain only one lattice site ($\lambda = 1$), whereas the unit cell of the *kagomé* lattice contains three sites ($\lambda = 3$).

Unlike the square or triangular lattice, the *kagomé* lattice is not a Bravais lattice. The *kagomé* is equivalent to a rhombic lattice with a three-point basis (Fig. 2). Basis points for the *kagomé* lattice are distinguished by the labels 1, 2, and 3, and are labeled by the indices α, β in (2.2); this index is extraneous for the square and triangle.

The Hamiltonian (2.2) has been well studied,[28–30] and in reciprocal space becomes

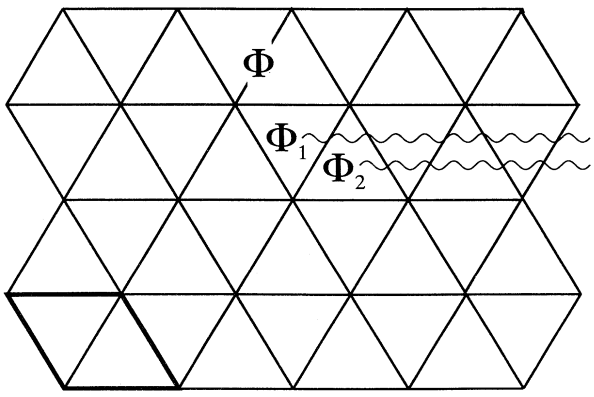

FIG. 1. The triangular lattice is shown with the rhombic unit cell outlined in the lower left corner. The flux per unit cell is the sum of the plaquette fluxes Φ_1 and Φ_2 through triangles of different orientation. Strings emanating from each plaquette illustrate the choice of gauge.

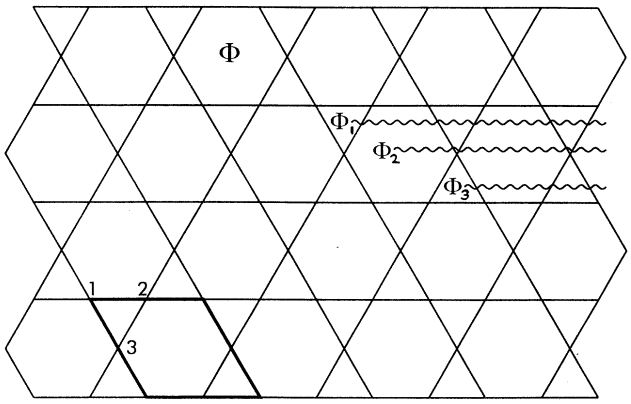

FIG. 2. The *kagomé* lattice is shown with the rhombic unit cell outlined in the lower left corner. The flux per unit cell is the sum of the triangular plaquette fluxes Φ_1 and Φ_3 and hexagonal plaquette flux Φ_2. The *kagomé* lattice is equivalent to a rhombic lattice with a three-point basis. Basis points are distinguished by the labels 1,2,3.

$$H = \frac{1}{(2\pi)^2}\int_0^{2\pi} dk_x \int_0^{2\pi} dk_y H(k_x, k_y), \tag{2.6}$$

where $H(k_x, k_y)$ is lattice dependent. Given a fraction of flux per unit cell $\Phi/\phi_0 = P/Q$, in order to satisfy the requirements of the magnetic translation group, the Brillouin zone must become Q-fold smaller in one direction, chosen to be the x direction. The eigenstate of $H(k_x, k_y)$ can therefore be written

$$|\psi\rangle = \sum_{j=1}^{Q} \psi_{j,\alpha} c_\alpha^\dagger \left(k_x^\circ + 2\pi\frac{P}{Q}j, k_y\right)|0\rangle, \tag{2.7}$$

where $k_x^\circ + 2\pi\frac{P}{Q}j$ replaces k_x, and (k_x°, k_y) are defined in the magnetic Brillouin zone $0 \le k_x^\circ \le 2\pi/Q$ and $0 \le k_y \le 2\pi$. The wave function $\psi_{j,\alpha}$ satisfies the "magnetic boundary condition" $\psi_{j+Q,\alpha} = \psi_{j,\alpha}$.

The eigenvalue equation $H(k_x, k_y)|\psi\rangle = E|\psi\rangle$ for the square lattice yields

$$\sum_{j=1}^{Q}\{[2\cos(k_x^\circ + 2\pi\Phi j/\phi_0) + E]\psi_j + e^{-ik_y}\psi_{j+1} + e^{ik_y}\psi_{j-1}\} = 0. \tag{2.8}$$

The difference equation (2.8) is known as Harper's equation. It was shown by Hofstadter[28] that the highly degenerate tight-binding band which results in the absence of a field is split into Q subbands for flux per unit cell $\Phi = \phi_0 P/Q$.

The unit cell for the triangular lattice is chosen to be the rhombus shown in the bottom left corner of Fig. 1. It is evident that two of the nearest-neighbor links do not follow primitive vectors, but are linear combinations of them. There is therefore some freedom in how the gauge field is defined along these links, as long as each unit cell encloses Φ flux. This freedom is parametrized by the fluxes Φ_1 and Φ_2 through the two triangular plaquettes comprising the rhombus, as shown in Fig. 1. The difference equation for the triangular case is then

$$\sum_{j=1}^{Q}\{[2\cos(k_x^\circ + 2\pi\Phi j/\phi_0) + E]\psi_j + [e^{\frac{i}{2}(k_x^\circ - \sqrt{3}k_y)} + e^{-\frac{i}{2}(k_x^\circ + \sqrt{3}k_y)}e^{-i2\pi\Phi(j+1)/\phi_0}e^{i2\pi\Phi_1/\phi_0}]\psi_{j+1} + [e^{-\frac{i}{2}(k_x^\circ - \sqrt{3}k_y)} + e^{\frac{i}{2}(k_x^\circ + \sqrt{3}k_y)}e^{i2\pi\Phi j/\phi_0}e^{-i2\pi\Phi_1/\phi_0}]\psi_{j-1}\} = 0, \tag{2.9}$$

where use has been made of the identity $\Phi_1 + \Phi_2 \equiv \Phi$. As in the square case, the single tight-binding band is split into Q magnetic subbands for flux per unit cell $\Phi = \phi_0 P/Q$.

In the case of the *kagomé lattice*, the unit cell is also chosen to be a rhombus, shown on the bottom left corner of Fig. 2. As in the triangular case, there are lattice links other than the primitive vectors. Thus again, there will be different possible mean-field solutions. These can be parametrized by the fluxes Φ_1, Φ_2, and Φ_3 through the triangular and hexagonal plaquettes comprising the rhombus, subject to the constraint that each unit cell has flux $\Phi = \Phi_1 + \Phi_2 + \Phi_3 = 3\phi_0(1-\nu)\rho$. Due to the summation over basis points, three equations are obtained:

$$\sum_{j=1}^{Q}\{E\psi_{j,1} + (1 + e^{i(k_x^\circ + 2\pi\Phi j/\phi_0)})\psi_{j,2} + \psi_{j-1,3} + e^{\frac{i}{2}(k_x^\circ - \sqrt{3}k_y)}\psi_{j,3}\} = 0,$$

$$\sum_{j=1}^{Q}\{(1 + e^{-i(k_x^\circ + 2\pi\Phi j/\phi_0)})\psi_{j,1} + E\psi_{j,2} + e^{-i2\pi\Phi_1/\phi_0}\psi_{j-1,3} + e^{-\frac{i}{2}(k_x^\circ + \sqrt{3}k_y)}e^{-i2\pi(\Phi j + \Phi_3)/\phi_0}\psi_{j,3}\} = 0,$$

$$\sum_{j=1}^{Q}\{\psi_{j+1,1} + e^{-\frac{i}{2}(k_x^\circ - \sqrt{3}k_y)}\psi_{j,1} + e^{i2\pi\Phi_1/\phi_0}\psi_{j+1,2} + e^{\frac{i}{2}(k_x^\circ + \sqrt{3}k_y)}e^{i2\pi(\Phi j + \Phi_3)/\phi_0}\psi_{j,2} + E\psi_{j,3}\} = 0. \tag{2.10}$$

For general flux per unit cell $\Phi = \phi_0 P/Q$ the number of subbands is $3Q$.

B. TKNN integer and superfluidity

It can be easily shown that the Hall conductance is quantized whenever the Fermi energy E_F lies in a gap between subbands. Each tight-binding band is split into λQ subbands for flux per unit cell $\Phi = \phi_0 P/Q$. If the particle density is such that the Fermi energy lies in a gap between subbands, then there will be f filled bands below E_F. The integers P, Q, and f satisfy the Diophantine equation:[25]

$$f = Qs_f + \lambda P t_f, \tag{2.11}$$

where s_f and t_f are unconstrained integers. The density of states $\mathcal{N}$ is equal to the fraction of filled subbands: $\mathcal{N} = f/\lambda Q$. Furthermore, the Středa formula[31] for the transverse Hall current is

$$\sigma_{xy} = ec\frac{\partial \mathcal{N}}{\partial B} = ec\frac{\partial \mathcal{N}}{\partial\left(\frac{hc}{e}\frac{P}{Q}\right)} = \frac{e^2}{h}t_f. \tag{2.12}$$

Since each t_f must be an integer, the Hall conductance for each subband is quantized in integer multiples of e^2/h.

The integers t_f are often called TKNN integers after Thouless *et al.*[25] The TKNN integer is a topological invariant,[26] and therefore the Hall conductance is insensitive to changes in the external flux as long as the gap between subbands remains well defined. The topological invariance is used in the calculation of the integers t_f and s_f associated with each gap.

The consideration of fluctuations about the mean-field configuration[17,18] yields the following condition on the integers t_f and s_f if the ground state of the system is a superfluid:

$$(t_f, s_f) = \left(\frac{1}{1-\nu}, 0\right). \tag{2.13}$$

Thus, semions on a lattice form a superfluid only if the density is such that E_F lies in a gap between subbands with the quantum numbers (2,0). Otherwise, the system is a quantum Hall insulator.[17] Since t_f must be an integer, the condition (2.13) implies that only anyons with the statistics

$$\nu = 1 - \frac{1}{n}, \quad n = 1, 2, 3, \ldots \tag{2.14}$$

can form a superfluid. These are the same statistics found by Fetter, Hanna, and Laughlin[11] and Chen *et al.*[12] to yield superfluidity for anyons in the continuum.

III. MEAN-FIELD RESULTS

A. Square

The energy spectrum for the square lattice, determined by the Harper equation (2.8), was analyzed by Hofstadter.[28] The TKNN integers were previously calculated by Hatsugai and Kohmoto.[32] Fradkin[17] has quantified the density constraints on superfluidity: given statistics $\nu = 1 - 1/n$ and density $\rho = r/q$, where r and q have no common factors, q must be greater than twice the common factor of n and r in order to ensure a superfluid state. For semions, this implies that all densities should form a superfluid except the cases $\rho = 1/2$ and $2/3$. The technique itself is not applicable to the case of half-filling, however, since the associated mean-field gap closes. A different analysis is necessary in order to determine whether the system at half-filling forms a superfluid.

B. Triangle

The energy-flux spectrum for anyons on the triangle is determined by the difference equation (2.9). The band structure is sensitive to the plaquette distribution of flux, parametrized by the flux Φ_1 through one of the two triangles comprising the unit cell. In order to determine which configuration the system favors, the total ground-state energy for semions at various densities is computed with Φ_1 as a parameter. The total energy is calculated by integrating over occupied states up to the Fermi level defined by the particle density. A calculation of the total energy based on the density of states[33,34] is not as practical for semions at densities other than half-filling due to the large number of subbands.

The total ground-state energies for semions on the triangle were calculated for densities $\rho = r/q$, $q = 2, 3, \ldots, 15$. For each density, flux fractions Φ_1/Φ with denominator 120 were considered. It is found that semions on the triangle have a lower total ground-state energy for the following, density-dependent, plaquette configuration of flux:

$$\Phi_1/\Phi = \begin{cases} 1/2, & \rho \le 1/2; \\ 0 \text{ or } 1, & \rho > 1/2. \end{cases} \tag{3.1}$$

Notable exceptions to this general observation are the densities $\rho = j/(j+1)$ with $j \ge 5$, which minimize the ground-state energy for semions when $\Phi_1/\Phi = 1/2$. No other plaquette flux distribution was found to minimize the total energy. The energy-flux spectra for the cases of uniform flux (equal flux fraction per plaquette) and staggered flux (all the flux in one of the triangular plaquettes) are shown in Figs. 3 and 4, respectively.

The topology of the energy-flux spectrum for the uniform case is such that the criterion for superfluidity (2.13) would be satisfied for semions at *any* density if this configuration of flux were energetically favorable. Semions at densities $\rho > 1/2$ generally prefer the staggered flux distribution, however. The result is a quantum Hall in-

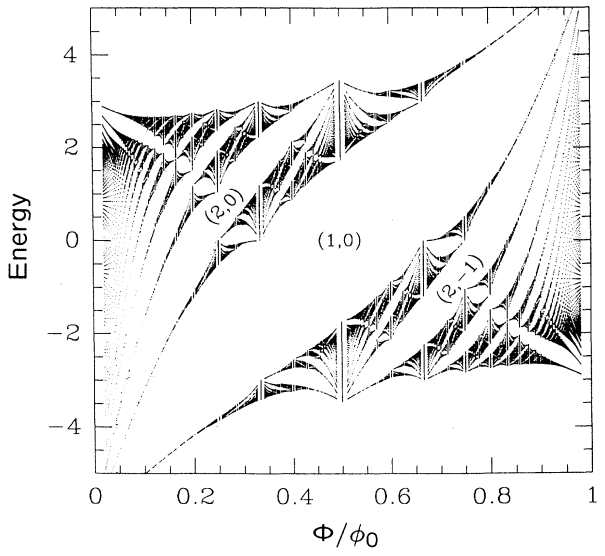

FIG. 3. The energy spread of the fermion subbands is given as a function of the flux fraction per unit cell $\Phi/\phi_0 = P/Q$ for the triangular lattice with an equal amount of flux in each plaquette. This configuration is favored when the semion density $\rho \leq 1/2$. Integers in the gaps are the topological invariants (t_f, s_f).

sulating state for semions at $\rho = 2/3$, as was found for semions on the square lattice, but a superfluid for all other densities.

C. *Kagomé*

The procedure for the determination of superfluid states for semions on the *kagomé* lattice proceeds analogously to that used for semions on the square and triangular lattices. In this case, the freedom in the distribution of the flux within a unit cell is parametrized by the fluxes Φ_1 and Φ_3 through the two triangular plaquettes. All flux fractions Φ_1/Φ and Φ_3/Φ with denominator 120 are tested in order to determine the lowest ground-state energy for a given semion density $\rho = r/q$ with $q = 2$ through 7. In general, the following configuration of plaquette flux is found to minimize the ground-state energy:

$$\Phi_1/\Phi = \Phi_3/\Phi = \begin{cases} 0, & \rho \leq 1/2; \\ 1/2, & \rho > 1/2. \end{cases} \tag{3.2}$$

The general trend given above is exactly satisfied for densities $\rho \leq 1/2$. For densities greater than half-filling, a number of exceptions are found; semions at the densities 3/4, 4/5, and 6/7 favor the flux distribution given by $\Phi_1/\Phi = \Phi_3/\Phi = 2/5$. The energy-flux spectra for the cases $(\Phi_1/\Phi, \Phi_3/\Phi) = (0,0)$, $(1/2, 1/2)$, and $(2/5, 2/5)$ are shown in Figs. 5, 6, and 7, respectively. It is curious to note that neither the case of uniform flux $(\Phi_1 = \Phi_2 = \Phi_3 = \Phi/3)$ nor the case $\Phi_1 = \Phi_3 = \Phi/8$, where the amount of flux per plaquette is proportional to its area, is an energetically favored configuration.

Semions on the *kagomé* were found to satisfy the criterion for superfluidity (2.13) for most densities studied in the regime $\rho \leq 1/2$. Exceptions are the case $\rho = 1/3$, a density for which the gap between subbands closes at the Fermi energy, and the cases $\rho = 2/9$ and $\rho = 4/9$, which have a Fermi energy located in gaps labeled by the integers $(-1,1)$ and $(-1,2)$ respectively. None of the densities $\rho > 1/2$ examined were found to yield superfluid states; for the majority of densities in this regime the integers t_f and s_f were not found to be (2,0). Semions on the *kagomé* at the densities $\rho = 3/4$ and $\rho = 3/5$ have a Fermi energy

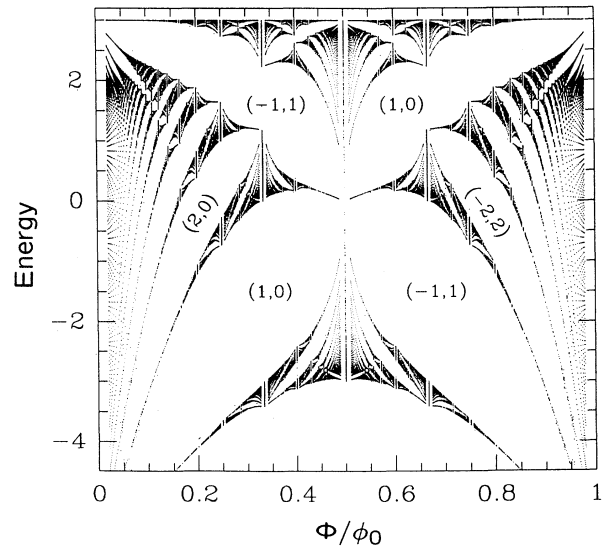

FIG. 4. The energy-flux diagram is given for the triangular lattice with an uneven flux distribution, i.e., when all of the flux is in one of the two plaquettes. Integers in the gaps are the topological invariants (t_f, s_f).

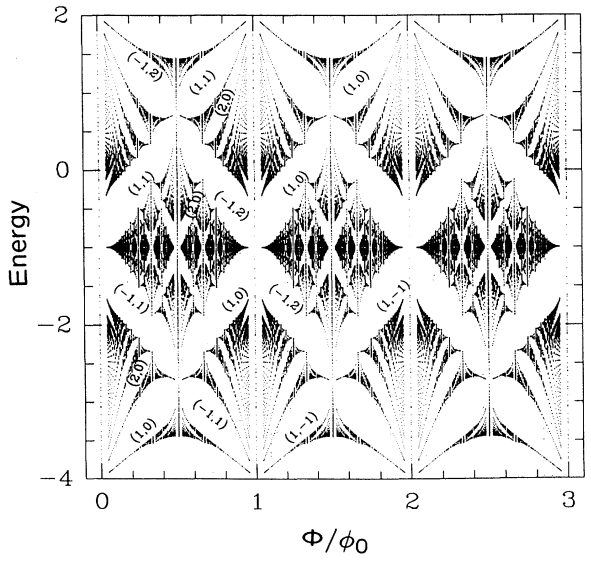

FIG. 5. The energy-flux diagram for the *kagomé* lattice is given with a plaquette flux distribution $\Phi_1/\Phi = \Phi_3/\Phi = 0$. This configuration is always favored for semion densities $\rho \leq 1/2$. Integers in the gaps are the topological invariants (t_f, s_f).

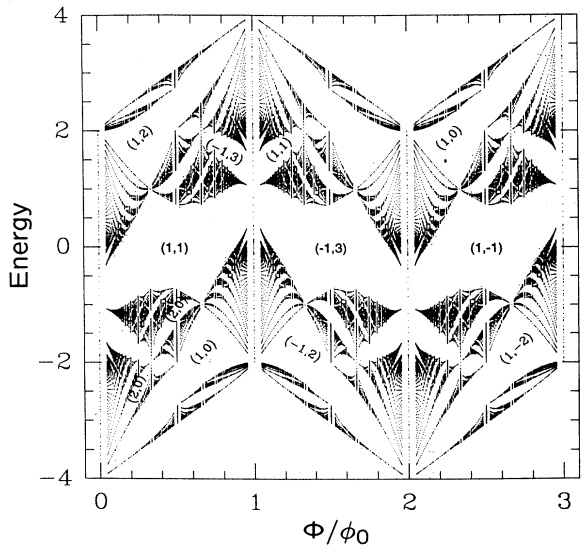

FIG. 6. The energy-flux diagram for the *kagomé* lattice is given with a plaquette flux distribution $\Phi_1/\Phi = \Phi_3/\Phi = 1/2$. Integers in the gaps are the topological invariants (t_f, s_f).

just at the point where two subbands meet, and therefore the theory can make no prediction about the nature of the ground state in these cases. No definitive statement can be made about the ground state for semions on the *kagomé* at densities greater than half-filling, however. Such a statement would require an exhaustive investigation of the preferred subplaquette flux configuration for any given density, and of the restrictions on semion superfluid states imposed by the topology of the resultant energy-flux spectrum.

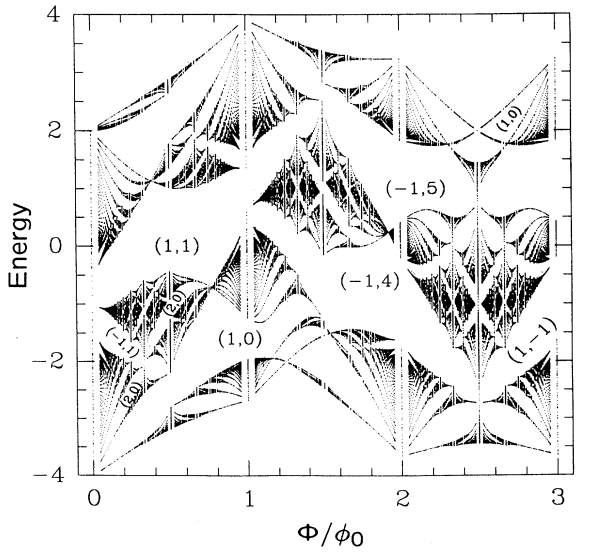

FIG. 7. The energy-flux diagram for the *kagomé* lattice is given with a plaquette flux distribution $\Phi_1/\Phi = \Phi_3/\Phi = 2/5$. Integers in the gaps are the topological invariants (t_f, s_f).

IV. NUMERICAL TECHNIQUE

Semions on a lattice with periodic boundary conditions in both directions are considered. Semions are represented by hard-core bosons with fictitious charge and flux $\phi_0/4$. The usual tight-binding Hamiltonian is employed:

$$H = -\sum_{\langle ij\rangle\alpha,\beta} T_{ij}\tilde{b}^{\dagger}_{j,\beta}\tilde{b}_{i,\alpha} + \text{H.c.} \tag{4.1}$$

The operator $\tilde{b}^{\dagger}_{j\alpha}$ ($\tilde{b}_{j\alpha}$) creates (destroys) a boson-gauge field composite at site j and basis point α, and the sum is over nearest neighbors as well as basis points $\alpha, \beta = a, b,$ or c. The hopping term T_{ij} includes the energy scale t (taken to be unity), the Aharonov-Bohm phases due to other particles, and the 2×2 matrices T_x and T_y imposed by considerations of the braid group[35] for anyons on the torus.[36] The matrices T_x and T_y, included whenever a semion crosses the lattice boundary in the positive $\hat{x}$ and $\hat{y}$ directions, respectively, anticommute[27,36] and are chosen such that the ground-state energy is a minimum with zero applied flux:

$$T_x = \begin{pmatrix} 1 & 0 \\ 0 & -1 \end{pmatrix}, \qquad T_y = \begin{pmatrix} 0 & i \\ i & 0 \end{pmatrix}. \tag{4.2}$$

The braid group for anyons on the torus with statistics $\nu = m/n$ stipulates that the eigenfunctions of (4.1) must have n components, and that the number of anyons must be a multiple of n. The Hilbert space is therefore n-fold larger for anyons than it is for fermions or bosons. Individual N-semion states can be written

$$|\psi\rangle = |S\rangle\sigma, \tag{4.3}$$

where $|S\rangle$ labels one of the ways N semions can occupy the sites of a lattice with R rows and C columns. The two-component spinor σ labels the two different "sheets": $\sigma = \binom{1}{0}$ and $\binom{0}{1}$. The sheet index can change only if the particle crosses a boundary.

Semions on the square (Fig. 8), triangle (Fig. 9), and *kagomé* (Fig. 10) are studied. Lattices with four semions on nine sites (square and triangle) and four semions on twelve sites (*kagomé*) are shown in the corresponding figures. Periodic boundary conditions are applied in both directions; lattices are bordered by "branch cuts" A and B which correspond to hops across the boundary in the $\hat{y}$ and $\hat{x}$ directions, respectively. Branch cuts are appropriately named — hops across them can induce phases as well as change the sheet index of the eigenstate.

The "string gauge" is employed;[23] the statistical potential is zero everywhere except along δ-function strings, which emanate from the particles, follow the y axis until almost reaching the lower branch cut A, turn abruptly to the right, and follow the x axis until terminating on the rightmost cut B. The magnitude of the vector potential along these strings is $\phi_0/4$ if the string is parallel to the y axis, and is $\phi_0/2$ if parallel to the x axis.

The hopping terms T_{ij} associated with the hops h for semions on the square, triangular, and *kagomé* lattices are given below. In occupation number formalism, $N_i^{>}$

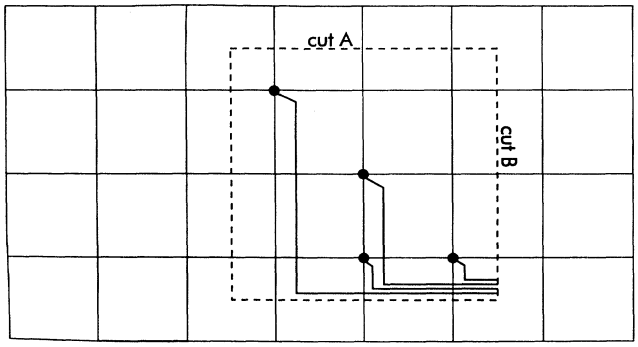

FIG. 8. Four anyons are placed on a 3×3 square lattice. Anyons are represented by hard-core bosons (circles) coupled to a vector potential in the string gauge. The strings emanate from the particles and terminate in the lower-right corner of the lattice. The lattice boundaries are labeled by the branch cuts A and B.

$(N_i^<)$ is defined as the number of particles with the same x coordinate as the hopping particle, but with a larger (smaller) y coordinate; N_i^- is the number of particles with a smaller x coordinate than that of the hopping particle, independent of their y coordinate; N_i° is the number of particles in the same column as, but not including, the hopping particle. The site label i is not sufficient to label occupied sites on the *kagomé*, since each lattice site has a three-point basis. All of the above definitions hold, with the appropriate modifications. For example, $N_{ib}^\geq$ is defined as the number of particles occupying b sites with the same x coordinate as the hopping particle but with a larger or equal y coordinate (not including the hopping particle itself).

The x and y coordinates have the following range (counted from the lower left corner of the lattice):

$$1 \leq x_i \leq C \quad , \quad 1 \leq y_i \leq R. \tag{4.4}$$

The symbols x_i and y_i represent the x and y coordinates of the ith site, respectively. Thus $x_i + \hat{x} > C$ means that the hop in the positive $\hat{x}$ direction has crossed cut B. Since the x and y axes are not perpendicular in the cases of the triangle and *kagomé*, a hop denoted by $h = \hat{x} + \hat{y}$ moves the particle to the nearest-neighbor site in a diagonal direction positive in *both* $\hat{x}$ and $\hat{y}$.

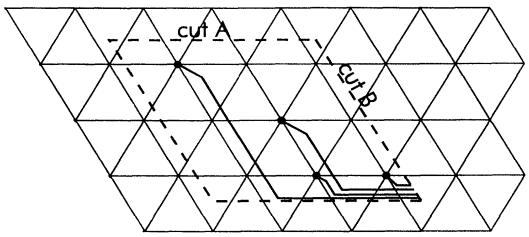

FIG. 9. The triangular lattice is shown with four particles and nine sites. Hard-core bosons are coupled to infinitesimal strings which carry the vector potential. The lattice is bounded by the cuts A and B.

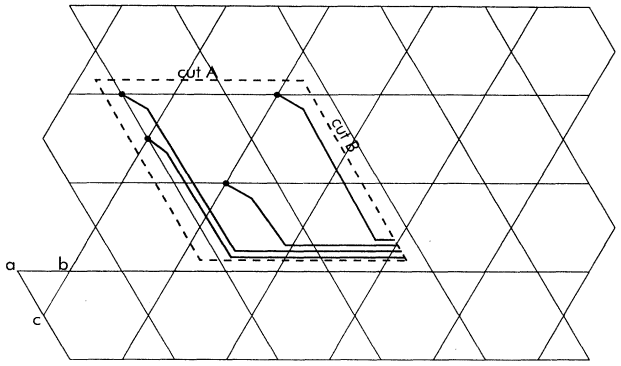

FIG. 10. The *kagomé* lattice is shown with four particles and twelve sites. Basis points are labeled a, b, or c depending on the nearest-neighbor environment. Branch cuts A and B denote the lattice boundaries.

A. Square

The nearest-neighbor links for the square lattice are $h = \hat{x}$ and $h = \hat{y}$. There are four cases, previously considered by Kallin:[23]
(i) $h = \hat{x}$; $x_i + \hat{x} \leq C$:

$$T_{ij} = \exp\left[i\pi\left(N_i^> - N_j^<\right)/2\right] I, \tag{4.5}$$

where I is the identity matrix of order 2.
(ii) $h = \hat{x}$; $x_i + \hat{x} > C$:

$$T_{ij} = \exp\left[i\pi\left(N_i^> - N_j^<\right)/2 + i2\pi\Phi_x/\phi_0\right] T_x, \tag{4.6}$$

where Φ_x is an external flux coincident with cut B included in order to test for flux quantization. It is evident from (4.6) that all energies are π-periodic in external flux; shifting Φ_x by $\phi_0/2$ is equivalent to interchanging the sheet indices, an operation which has no effect on the energies.
(iii) $h = \hat{y}$; $y_i + \hat{y} \leq R$: $T_{ij} = I$.
(iv) $h = \hat{y}$; $y_i + \hat{y} > R$:

$$T_{ij} = \exp\left[i\pi\left(2N_i^- + N_i^\circ\right)/2 + i2\pi\Phi_y/\phi_0\right] T_y, \tag{4.7}$$

where Φ_y is an external flux felt by particles crossing cut A. External fluxes are included in both directions in order to find the absolute minimum of energy as well as to check the rotational invariance of the results. The term N_i° in the definition of the hopping matrix ensures the correct ordering of strings; when a particle-string composite crosses cut A, the horizontal component of its string is incorrectly ordered with respect to the strings of the particles to its right.

B. Triangle

If the x and y axes are parallel to the basis vectors then semions on the triangular and square lattices give the same phases for the hops $h = \hat{x}$ and $\hat{y}$. Accordingly, cases (i) through (iv) listed above are also applicable to hops on

the triangle. Semions on the triangle have an additional nearest-neighbor hop: $h = \hat{x} + \hat{y}$, which corresponds to the following cases:
(v) $h = \hat{x} + \hat{y}$; $x_i + \hat{x} \leq C$; $y_i + \hat{y} \leq R$:

$$T_{ij} = \exp\left[i\pi\left(N_i^{>} - N_j^{<}\right)/2\right] I, \tag{4.8}$$

which is identical to case (i) except that here $y_j = y_i + 1$.
(vi) $h = \hat{x} + \hat{y}$; $x_i + \hat{x} > C$; $y_i + \hat{y} \leq R$:

$$T_{ij} = \exp\left[i\pi\left(N_i^{>} - N_j^{<}\right)/2 + i2\pi\Phi_x/\phi_0\right] T_x. \tag{4.9}$$

(vii) $h = \hat{x} + \hat{y}$; $x_i + \hat{x} \leq C$; $y_i + \hat{y} > R$:

$$T_{ij} = \exp\left[i2\pi\left(N_j^{-}/2 + \Phi_y/\phi_0\right)\right] T_y. \tag{4.10}$$

Note that the factor N_j° necessary to account for the correct ordering of strings as in case (iv) does not appear.
(viii) $h = \hat{x} + \hat{y}$; $x_i + \hat{x} > C$; $y_i + \hat{y} > R$:

$$T_{ij} = \exp\left[i2\pi\left(\Phi_x + \Phi_y\right)/\phi_0\right] T_y T_x \tag{4.11}$$

$$= \exp\left[i\pi\left(N-1\right) + i2\pi\left(\Phi_x + \Phi_y\right)/\phi_0\right] T_x T_y, \tag{4.12}$$

where the equivalence of (4.11) and (4.12) is proven by making use of the braid group condition that only an even number of semions is allowed on the torus.

C. *Kagomé*

Since each lattice point of the *kagomé* is associated with three basis points, the nearest-neighbor hops are basis dependent.
(i) $h = \hat{x}$; $a \rightarrow b$:

$$T_{ij} = \exp\left[i\pi\left(N_{ia}^{>} + N_{ic}^{>} - N_{ib}^{<}\right)/2\right] I. \tag{4.13}$$

(ii) $h = \hat{x}$; $b \rightarrow a$; $x_{ib} + \hat{x} \leq C$:

$$T_{ij} = \exp\left[i\pi\left(N_{ib}^{>} - N_{ja}^{<} - N_{jc}^{\leq}\right)/2\right] I. \tag{4.14}$$

Note that account must be taken of the string crossing a particle on basis point c of the *same* lattice point j.
(iii) $h = \hat{x}$; $b \rightarrow a$; $x_{ib} + \hat{x} > C$:

$$T_{ij} = \exp\left[i\pi\left(N_{ib}^{>} - N_{ja}^{<} - N_{jc}^{\leq}\right)/2 + i\,2\pi\Phi_x/\phi_0\right] T_x. \tag{4.15}$$

(iv) $h = \hat{y}$; $c \rightarrow a$: $T_{ij} = I$.
(v) $h = \hat{y}$; $a \rightarrow c$; $y_{ia} + \hat{y} \leq R$: $T_{ij} = I$.
(vi) $h = \hat{y}$; $a \rightarrow c$; $y_{ia} + \hat{y} > R$:

$$T_{ij} = \exp\left[i\pi\left(2N_i^{-} + N_{ia}^{\circ} + N_{ic}^{\circ}\right)/2 + i\,2\pi\Phi_y/\phi_0\right] T_y. \tag{4.16}$$

(vii) $h = \hat{x} + \hat{y}$; $c \rightarrow b$:

$$T_{ij} = \exp\left[i\pi\left(N_{ia}^{\geq} + N_{ic}^{>} - N_{ib}^{<}\right)/2\right] I. \tag{4.17}$$

(viii) $h = \hat{x} + \hat{y}$; $b \rightarrow c$; $x_{ib} + \hat{x} \leq C$; $y_{ib} + \hat{y} \leq R$:

$$T_{ij} = \exp\left[i\pi\left(N_{ib}^{>} - N_{ja}^{<} - N_{jc}^{<}\right)/2\right] I. \tag{4.18}$$

(ix) $h = \hat{x} + \hat{y}$; $b \rightarrow c$; $x_{ib} + \hat{x} > C$; $y_{ib} + \hat{y} \leq R$:

$$T_{ij} = \exp\left[i\pi\left(N_{ib}^{>} - N_{ja}^{<} - N_{jc}^{<}\right)/2 + i\,2\pi\Phi_x/\phi_0\right] T_x. \tag{4.19}$$

(x) $h = \hat{x} + \hat{y}$; $b \rightarrow c$; $x_{ib} + \hat{x} \leq C$; $y_{ib} + \hat{y} > R$:

$$T_{ij} = \exp\left[i2\pi\left(N_j^{-}/2 + \Phi_y/\phi_0\right)\right] T_y. \tag{4.20}$$

(xi) $h = \hat{x} + \hat{y}$; $b \rightarrow c$; $x_{ib} + \hat{x} > C$; $y_{ib} + \hat{y} > R$:

$$T_{ij} = \exp\left[i2\pi\left(\Phi_x + \Phi_y\right)/\phi_0\right] T_y T_x \tag{4.21}$$

$$= \exp\left[i\pi\left(N-1\right) + i2\pi\left(\Phi_x + \Phi_y\right)/\phi_0\right] T_x T_y\,. \tag{4.22}$$

D. Procedure

The computational time required to diagonalize the Hamiltonian (4.1) can be significantly reduced by making use of the discrete translational symmetry of the lattice. The Bloch states that usually diagonalize a lattice Hamiltonian must be modified in the anyon case due to the presence of the branch cuts A and B. In the present study, use is made of the translational symmetry of the lattice in both directions. The technique is described in detail in Ref. 23.

The computer programs used in the diagonalization of the Hamiltonian (4.1) are tested in three ways. First, the ground-state energies of spinless fermions on the lattices are tested by coupling hard-core bosons to strings with weight $\phi_0/2$. Second, the rotational symmetry of the torus implies that all energies should be invariant to the interchange of the fluxes Φ_x and Φ_y if the magnitudes of R and C are simultaneously interchanged. The third test, which checks the block diagonalization of the Hamiltonian and consequently the translational symmetry of the Bloch states, is perhaps the most stringent. The vanishing of all Hamiltonian matrix elements between states labeled by different $\mathbf{k}$ provides convincing evidence that the Bloch states[23] are correctly defined.

The ground-state energy for semions on the torus is $\phi_0/2$-periodic in external flux; this periodicity is the result of braid group considerations and is not indicative of flux quantization. Superfluid states can be monitored by investigating the scaling of the energy barrier, the difference between the maximum and adjacent minimum of energy, with system size. The energy barrier for a finite system can be written[37]

$$E\left(\Phi = \frac{\phi_0}{4}\right) - E(\Phi = 0) = \rho_s \frac{N}{\lambda R^2}\left(\frac{\pi}{2}\right)^2, \tag{4.23}$$

where ρ_s is the superfluid fraction. This equation is valid in the continuum limit but can be used to give a crude approximation of ρ_s for semions on a lattice. It is assumed that the external flux is along a single direction. For all the results presented below, $\Phi_x = 0$ and $\Phi_y = \Phi$.

The smallest square and triangular lattice studied had $R = C = 3$ (9 sites), while the smallest *kagomé* lattice had $R = C = 2$ (12 sites). No lattice was stud-

ied with fewer rows or columns in order to minimize finite-size effects. The largest lattices investigated had $R = C = 5$ (25 sites) and $R = C = 3$ (27 sites) for the square/triangle and *kagomé* lattices, respectively. The system with the largest Hilbert space was 8 semions on a *kagomé* lattice with 24 sites. By making use of the translational symmetry, the 1 470 942 states were reduced to 184 256. A Lanczos algorithm determined the ground-state energy.

V. NUMERICAL RESULTS

A. Square

The energy barrier for semions on the square has been computed for a variety of densities and lattice sizes. Semions do not have particle-hole symmetry; indeed, semions at density ρ have the same energy as semions at density $1 - \rho$ in a uniform field of magnitude $\phi_0/2$ per site. The flux quantization results for semions at the densities $\rho \leq 1/2$ and $\rho \geq 1/2$ are therefore considered separately.

The energy barrier for semions on the square at densities $\rho \leq 1/2$ (Fig. 11) is found to be a generally linear function of N/R^2, indicating that semions in this density regime form a superfluid. By contrast, there is no indication of flux quantization for semions at half-filling. This observation is in agreement with previous numerical investigations of semions on the square.[20,21] Note that mean-field theory can make no prediction about the semion ground state at this density due to the closure of the associated gap at the Fermi energy.

The roughly linear scaling of the energy barrier with N/R^2 for semions at densities $\rho \geq 1/2$, shown in Fig. 12, indicates that semions also exhibit flux quantization for most densities greater than half-filling. A notable exception to this general observation is the case of semions at $\rho = 2/3$; the absence of scaling of the energy barrier with N/R^2 corroborates the mean-field prediction that semions at this density form a quantum Hall insulator.

The scaling of the energy barrier with the number of particles observed for semions on the square is not simply a finite-size effect. For example, the semion flux quantization curves are in striking contrast with what is observed for noninteracting fermions on the same small lattices (Fig. 13); the absence of any indication of flux quantization was found to persist in the thermodynamic limit. By contrast, small systems of lattice bosons are known to exhibit clear evidence of flux quantization,[21,38] in accordance with expectation.[39]

The increase in the size of the energy barrier with increasing C at constant R, such as observed at $N/R^2 = 0.25$ or near $N/R^2 = 0.4$ in Fig. 11, is either a finite-size or lattice effect. The scatter in the data points resulting from this artificial scaling is nevertheless a valuable indicator of the quality of the flux quantization signature. A crude estimate of the superfluid fraction from (4.23) yields $\rho_s^< = 0.50 \pm 0.03$ for semions at densities less than half-filling, and $\rho_s^> = 0.29 \pm 0.02$ for semions

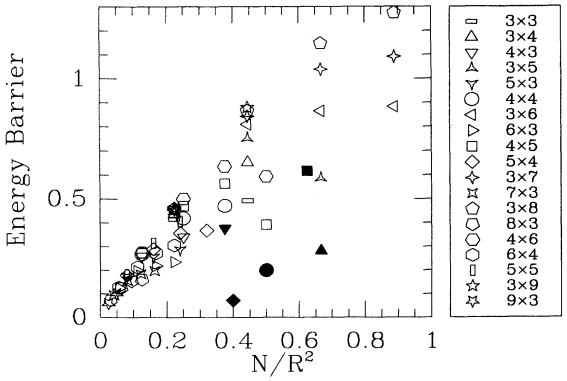

FIG. 11. The energy barrier $E(\Phi = \phi_0/4) - E(\Phi = 0)$ is given as a function of N/R^2 for semions on an $R \times C$ square lattice at densities $\rho \leq 1/2$. Filled points indicate semions at half-filling.

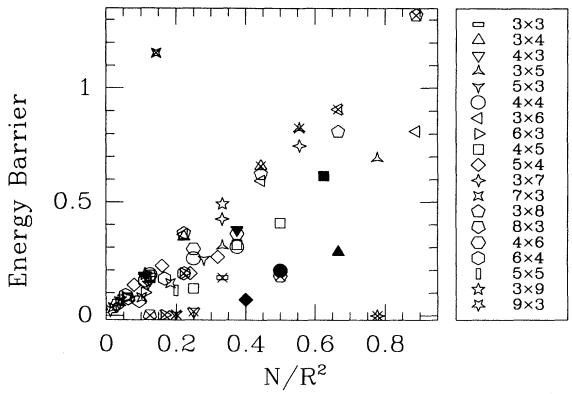

FIG. 12. The energy barrier $E(\Phi = \phi_0/4) - E(\Phi = 0)$ is given as a function of N/R^2 for semions on an $R \times C$ square lattice at densities $\rho \geq 1/2$. Filled points indicate semions with $\rho = 1/2$. Points with crosses correspond to $\rho = 2/3$; semions at this density are predicted by mean-field theory to be a quantum Hall insulator.

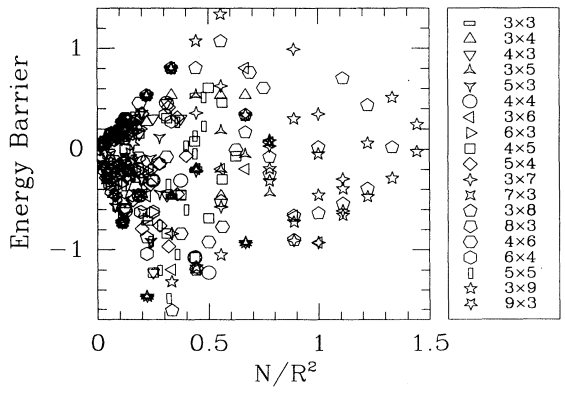

FIG. 13. The energy barrier for fermions, defined as $E(\Phi = \phi_0/4) - E(\Phi = 0)$ for comparison to the semion case, is given as a function of N/R^2 for the square lattice. Note that the "barrier" is equally likely to be negative as positive in this case, in stark contrast to the case of semions.

at densities greater than half-filling (if the points corresponding to the density $\rho = 2/3$ are neglected). The lower value of $\rho_s^>$ compared with that of $\rho_s^<$ may be due to frustration caused by the effective magnetic field induced on the transformation from particles to holes. It should be noted, however, that as the density approaches half-filling lattice effects become increasingly significant; Eq. (4.23) is only reliable for the near-continuum limit of very low densities.

B. Triangle

The flux quantization results for semions on the triangle at densities $\rho \leq 1/2$, shown in Fig. 14, are remarkably similar to those for semions on the square in this density regime (Fig. 11). Semions are found to exhibit flux quantization for all densities less than half-filling, and for most densities $\rho \geq 1/2$. The results for semions on the triangle differ slightly from those for semions on the square for these densities, however.

The superfluid fraction for semions at less than half-filling is estimated from the data points in Fig. 14 to be $\rho_s^< = 1.00 \pm 0.05$. The larger superfluid fraction for semions on the triangle compared to that for semions on the square in the same density regime indicates that the triangle is more conducive to semion superfluid states. This can be understood in a mean-field context by noting that the gaps labeled by the integers (2,0), which are the gaps of interest in the semion case, are generally larger for the triangle (Figs. 3 and 4) than are the corresponding mean-field gaps for the square;[28] this stabilizes the state against quasiparticle excitations.

There is considerably less scatter in the data points corresponding to semions at half-filling than was found for semions at this density on the square. However, the positions and the small slope of the points give an ambiguous indication of flux quantization. This result may be a reflection of the competing mean-field solutions for semions on the triangular lattice at this density; the mean-field calculation of the total energy per site yielded

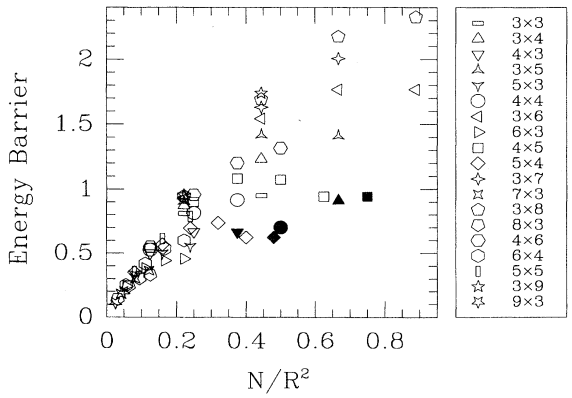

FIG. 14. The energy barrier $E(\Phi = \phi_0/4) - E(\Phi = 0)$ is given as a function of N/R^2 for semions on an $R \times C$ triangular lattice at densities $\rho \leq 1/2$. Filled points indicate semions at half-filling.

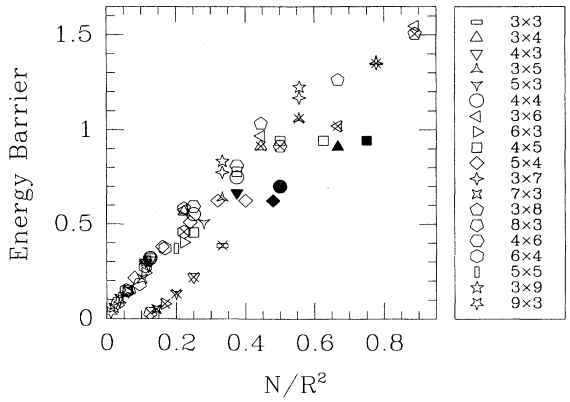

FIG. 15. The energy barrier $E(\Phi = \phi_0/4) - E(\Phi = 0)$ is given as a function of N/R^2 for semions on an $R \times C$ triangular lattice at densities $\rho \geq 1/2$. Filled points indicate semions with $\rho = 1/2$. Points with crosses correspond to $\rho = 2/3$; semions at this density are predicted by mean-field theory to be a quantum Hall insulator.

-1.044 for the staggered case and -1.049 for the uniform case.

The results for semions on the triangle at densities $\rho \geq 1/2$ are shown in Fig. 15. The energy barrier is found to be a monotonically increasing function of N/R^2 for virtually all densities examined. Notable exceptions to this general observation are the data points corresponding to $\rho = 2/3$; while these points scale in the appropriate manner, their overall shift to the right indicates that this density is special. This observation is also consistent with the mean-field analysis of semions on the triangle, which predicts an insulating state for semions at 2/3 filling. The large slope and virtual colinearity of the remaining data points indicate that semions at all other densities $\rho > 1/2$ form a superfluid.

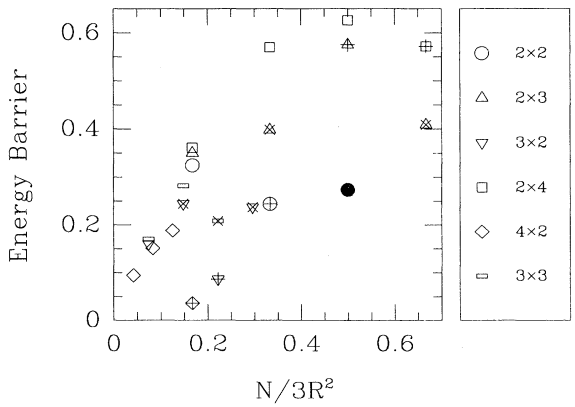

FIG. 16. The energy barrier $E(\Phi = \phi_0/4) - E(\Phi = 0)$ is given as a function of $N/3R^2$ for semions on an $R \times C$ *kagomé* lattice at densities $\rho \leq 1/2$. Points marked with a "×" label densities $\rho = 2/9$ and $4/9$; mean-field theory predicts that semions at these densities are insulating. Points with a "+" correspond to $\rho = 1/3$, which is associated with the closure of the mean-field gap at the Fermi energy. The solid point corresponds to half-filling.

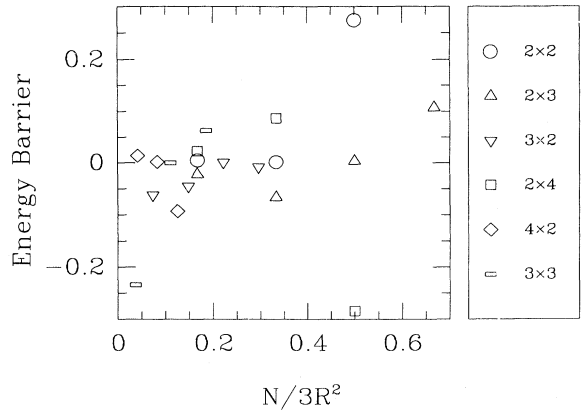

FIG. 17. The energy barrier $E(\Phi = \phi_0/4) - E(\Phi = 0)$ is given as a function of $N/3R^2$ for semions on an $R \times C$ *kagomé* lattice at densities $\rho \geq 1/2$. No semion densities are predicted by mean-field theory to support a superfluid state.

C. *Kagomé*

The flux quantization results for semions on the *kagomé* lattice are shown in Fig. 16 ($\rho \leq 1/2$) and Fig. 17 ($\rho \geq 1/2$). Though the number of data points is necessarily limited, the results of the finite-size study suggest that only semion densities less than half-filling support superfluid states on the *kagomé*. No evidence of flux quantization is observed for densities $\rho > 1/2$, in accordance with the mean-field predictions. While the apparent existence of many low-lying or degenerate states in this density regime makes the Lanczos algorithm for the determination of the ground-state energies less reliable, the lack of any scaling of the points shown in Fig. 17 unequivocally indicates nonsuperfluid states.

The majority of the data points for densities $\rho \leq 1/2$ scale linearly with $N/3R^2$, in agreement with the mean-field analysis. No convincing scaling is found for the data points corresponding to the densities $\rho = 2/9$ or $4/9$, corroborating the mean-field prediction of a quantum Hall insulator for semions at these densities. The shift to the right of the points representing $\rho = 1/3$ also indicates a nonsuperfluid state; the corresponding mean-field theory yields a gap closure at the Fermi energy. The poor location of the data point corresponding to $\rho = 1/2$ in Fig. 16 may be a finite-size effect; one would expect a high degree of frustration associated with a 2×2 lattice at half-filling.

The superfluid fraction for densities less than half-filling estimated from the data points in Fig. 16 (omitting the points corresponding to $\rho = 1/3$, $2/9$, and $4/9$) is $\rho_s^< = 0.53 \pm 0.05$. It would appear, therefore, that semions in this density regime are less capable of forming a superfluid on the *kagomé* than they are on the triangle. This observation has its counterpart in the mean-field analysis. The gaps labeled by the integers (2,0) are considerably smaller for the *kagomé* than for the square and triangle, indicating that fluctuation effects could more easily overwhelm the superfluid state for semions on the *kagomé*.

VI. CONCLUSIONS

Semions at zero temperature on the square, triangular, and *kagomé* lattices have been investigated using a mean-field theory and a finite-size analysis. Semions on the square and triangle are found to form a superfluid for all densities $\rho < 1/2$, though several nonsuperfluid states result for densities $\rho \geq 1/2$. Semions on the *kagomé* are less capable of forming a superfluid at any density. While the density restrictions on semion superfluidity are mostly lattice dependent, semions at two-thirds filling are found to form an insulating ground state for all lattices. The results of the finite-size study also suggest that semions at half-filling may not form a superfluid state.

The complete parallel between the results of the mean-field and finite-size analyses of lattice semions lends credence to the efficacy of the mean-field approach for the prediction of anyon superfluid states. No doubt the long-range nature of the statistical interaction is largely responsible for the validity of the mean-field approach. A convincing flux quantization signature is only observed if the corresponding mean-field theory predicts a superfluid state. Furthermore, no strong evidence of flux quantization is found for semion densities (such as $\rho = 1/2$) that yield a closure of the associated mean-field gap at the Fermi energy. The overwhelming success of the mean-field theory in the prediction of semion superfluidity begs the question of the ground state for anyons with statistics other than those defined by the mean-field condition, $\nu = 1 - 1/n$; this question will be addressed in future work.

ACKNOWLEDGMENTS

The authors would like to thank S.M. Girvin for useful comments. This work was supported by the Fonds pour la Formation de Chercheurs et l'Aide à la Recherche and the Natural Sciences and Engineering Research Council of Canada.

[1] F. Wilczek, Phys. Rev. Lett. **48**, 1144 (1982).
[2] F. Wilczek, Phys. Rev. Lett. **49**, 957 (1982).
[3] D.C. Tsui, H.L. Stormer, and A.C. Gossard, Phys. Rev. Lett. **48**, 1559 (1982).
[4] R.B. Laughlin, Phys. Rev. Lett. **50**, 1395 (1983).
[5] B.I. Halperin, Phys. Rev. Lett. **52**, 1583; D. Arovas, J.R. Schrieffer, and F. Wilczek, *ibid.* **53**, 722 (1984).
[6] P.W. Anderson, Mater. Res. Bull. **8**, 153 (1973).
[7] V. Kalmeyer and R.B. Laughlin, Phys. Rev. Lett. **59**, 2095 (1987).
[8] S.E. Korshunov, Phys. Rev. B **47**, 6165 (1993).
[9] K. Yang, L.K. Warman, and S.M. Girvin, Phys. Rev. Lett.

70, 2641 (1993).
[10] X.-G. Wen, F. Wilczek, and A. Zee, Phys. Rev. B **39**, 11 413 (1989).
[11] A.L. Fetter, C.B. Hanna, and R.B. Laughlin, Phys. Rev. B **39**, 9679 (1989).
[12] Y.-H. Chen, F. Wilczek, E. Witten, and B.I. Halperin, Int. J. Mod. Phys. B **3**, 1001 (1989).
[13] R.B. Laughlin, Science **242**, 525 (1988); Phys. Rev. Lett. **60**, 2677 (1988).
[14] T.W. Lawrence, A. Szöke, and R.B. Laughlin, Phys. Rev. Lett. **69**, 1439 (1992)
[15] T. Hasegawa, M. Nantoh, S. Heike, A. Takagi, M. Ogino, M. Kawasaki, H. Koinuma, and K. Kitazawa, J. Phys. Chem. Solids **54**, 1351 (1993); Phys. Scr. **T49**, 215 (1993).
[16] K.B. Lyons, J.F. Dillon, Jr., S.J. Duclos, C.B. Eom, H.L. Kao, J. Kwo, J.M. Phillips, and M.P. Siegal, Phys. Rev. B **47**, 8195 (1993).
[17] E. Fradkin, Phys. Rev. B **42**, 570 (1990).
[18] F.C. Zhang and M.R. Norman, Phys. Rev. B **43**, 6143 (1991).
[19] G.S. Canright, S.M. Girvin, and A. Brass, Phys. Rev. Lett. **63**, 2291 (1989).
[20] G.S. Canright, S.M. Girvin, and A. Brass, Phys. Rev. Lett. **63**, 2295 (1989).
[21] W. Wu, C. Kallin, and A. Brass, Phys. Rev. B **42**, 2222 (1990).
[22] Y. Hatsugai, M. Kohmoto, and Y.-S. Wu, Phys. Rev. B **43**, 2661 (1991); Prof. Theor. Suppl. **107**, 101 (1992).
[23] C. Kallin, Phys. Rev. B **48**, 13 742 (1993).
[24] F. Wilczek and A. Zee, Phys. Rev. Lett. **51**, 2250 (1983); D.P. Arovas, R. Schrieffer, F. Wilczek, and A. Zee, Nucl. Phys. **B251**, 117 (1985).
[25] D.J. Thouless, M. Kohmoto, M.P. Nightingale, and M. den Nijs, Phys. Rev. Lett. **49**, 405 (1982).
[26] M. Kohmoto, Ann. Phys. (N.Y.) **160**, 343 (1985).
[27] T. Einarsson, Phys. Rev. Lett. **64**, 1995 (1990).
[28] D. Hofstadter, Phys. Rev. B **14**, 2239 (1976).
[29] G.H. Wannier, Phys. Status Solidi B **88**, 757 (1978).
[30] M. Kohmoto, Phys. Rev. B **39**, 11 943 (1989).
[31] P. Středa, J. Phys. C **15**, L1299 (1982).
[32] Y. Hatsugai and M. Kohmoto, Phys. Rev. B **42**, 8282 (1990).
[33] Y. Hasegawa, P. Lederer, T.M. Rice, and P. Wiegmann, Phys. Rev. Lett. **63**, 907 (1989).
[34] Y. Hasegawa, Y. Hatsugai, M. Kohmoto, and G. Montambaux, Phys. Rev. B **41**, 9174 (1990).
[35] J.S. Birman, Commun. Pure Appl. Math. **22**, 41 (1969).
[36] Y. Hatsugai, M. Kohmoto, and Y.-S. Wu, Phys. Rev. B **43**, 10 761 (1991).
[37] N. Byers and C.N. Yang, Phys. Rev. Lett. **7**, 46 (1961).
[38] D.L. Feder (unpublished).
[39] T. Kennedy, E.H. Lieb, and B.S. Shastry, Phys. Rev. Lett. **61**, 2582 (1988).